FLOW AROUND NONPARALLEL TANDEM CYLINDERS

Md. Yamin Younis
Institute for Turbulence-Noise-Vibration Interaction and Control
Shenzhen Graduate School, Harbin Institute of Technology
Shenzhen, 518055, China
younis.my@hitsz.edu.cn

Md. Mahbub Alam
Institute for Turbulence-Noise-Vibration Interaction and Control
Shenzhen Graduate School, Harbin Institute of Technology
Shenzhen, 518055, China
alam@hit.edu.cn; alamm28@yahoo.com

Yu Zhou
Institute for Turbulence-Noise-Vibration Interaction and Control
Shenzhen Graduate School, Harbin Institute of Technology
Shenzhen, 518055, China

ABSTRACT

Flow around two nonparallel tandem cylinders is investigated experimentally to understand the associated fluid dynamics at a Reynolds number $Re = 5.6 \times 10^4$. Two cylinders of identical diameter D are oppositely inclined by 7.5° measured from the normal to the free stream direction, which leads to an included angle of 15° between the cylinders. Strouhal number (St) and time-mean and instantaneous flow field measurements for L^* (= L/D = 1 - 4.05, where L is the cylinder center-to-center spacing) leads to identification of three distinct flows: alternating reattachment flow (regime I, $1 \leq L^* < 2.15$), bi-stable flow (regime II, $2.15 \leq L^* \leq 3.1$), and coshedding flow (regime III, $3.1 < L^* \leq 4.05$). Regime I is further subdivided into regimes IA and IB contingent on shear layer reattachment and its influence on quasi-steady vortex in the gap and wake. The three flow regimes are totally different from those for parallel cylinders. A spiral vortex forming in the gap that varies along the cylinder span is responsible for making the difference. The sporadic presence of reattachment and coshedding flows results in a jump in St at regime II. In contrast to parallel cylinders, nonparallel cylinders experience another jump in St associated with the coshedding flow at $L^* = 2.5$ in regime II. A wake-flow bifurcation at $L^* = 2.5$ is responsible for the jump, separating the wake flow turning towards the small L^* and towards the large L^*.

INTRODUCTION

Fluid dynamics around two parallel cylinders subjected to a cross-flow has long been a topic of interest in the fields of fluid mechanics and fluid-structure interactions. Investigations related to two parallel tandem cylinders (Igarashi 1981; Xu and Zhou 2004; Alam 2016) revealed various features of shear layers, vortex shedding and wake, depending on Re and spacing (L) between the cylinders. The flow in general is classified into three types based on L^*(= L/D), namely overshoot or extended-body flow ($1 < L^* < 1.2$ - 1.8), reattachment flow (1.2 - $1.8 < L^* < 3.4$ - 3.8), and coshedding flow ($L^* > 3.4$ - 3.8). The L^* range of each flow regime is dependent on Re and

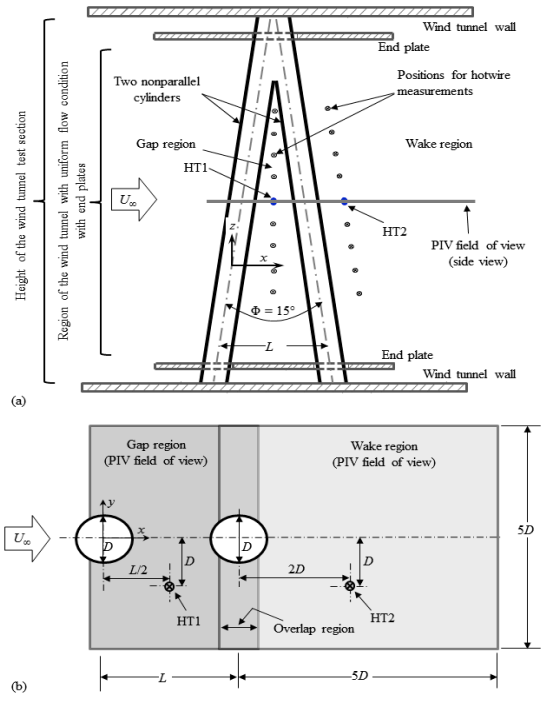

Figure 1. Experimental setup.

turbulent intensity (Sakamoto et al. 1987; Alam 2014). Alam et al. (2003) further divided the reattachment regime into alternating flow ($1.5 < L^* < 3$) and steady reattachment flow ($3 < L^* < 4$). The reattachment may occur on the front or rear side of the downstream cylinder depending on L^* and Re (Alam 2014). The L^* where flow changes from reattachment to co-shedding is known as critical spacing. Both flows may intermittently appear at the critical spacing.

For two nonparallel cylinders, continuously varying gap along the span upsurges the flow complexity, thus, may reveal fascinating new physics. For a yawed cylinder, the approaching flow can be decomposed into two components, perpendicular to and along the cylinder axis, respectively. The axial component, depending on the cylinder inclination, influences the wake substantially, forming a spanwise directed vortex pattern known as principal axial vortex (Ming et al. 2009). The principal axial vortex accelerates the vortex breakdown (Ming et al. 2009) resulting in a broadband frequency spectrum (Hogan and Hall 2011).

In the literature, the focus remained on the single or two parallel yawed cylinders arranged in tandem. The independence principle (IP) for a single yawed cylinder was found to be valid for yaw angle ≤ 45° (Najafi et al. 2016). Lam et al. (2012) observed that IP is valid for two tandem parallel cylinders for yaw angles between 0° to 30° for L^* = 1.5 - 5.5. For two nonparallel tandem cylinders, a number of questions may arise. Could we extrapolate the knowledge of the parallel cylinder wake for the nonparallel cylinder wake? How does the flow at large L^* interact with that at small L^*, and its effect on flow classification and St? Is the IP valid for the nonparallel cylinders? There are few studies on two tandem cylinders with one of them yawed (Stephen et al. 2013; Stephen and Joseph 2013). To understand the detailed flow physics and insight into the flow behaviour, a synthesized analysis of shedding frequency and flows on the cylinder surface, in the gap and in the wake would be very insightful.

This work aims to investigate the flow around two tandem nonparallel cylinders at a included angle $\Phi = 15°$. With a view to understanding the detailed flow physics, measurements of St, flow structures, flow field, flow separation angles, etc., are conducted using hotwire, PIV and surface oil-flow visualization techniques.

EXPERIMENTAL SETUP

Experiments were performed in a low-speed, closed-circuit wind tunnel, the arrangement of cylinders mounted vertically is shown in Fig. 1(a). The included angle Φ between the cylinders is 15°, leading to ±7.5° inclinations of two cylinders, respectively. The Re based on U_∞ and the cylinder diameter (D) was $Re = 5.6 \times 10^4$. The cylinder center-to-center spacing ratio $L^* \approx 1$, where two cylinders are joined together (Fig. 1(a)), is located at a distance of $0.177H$ from the upper-end plate (H is the height of the tunnel). The maximum spacing ratio investigated is L^* = 4.05 was $0.257H$ away from the lower-end plate.

The vortex shedding frequencies were estimated from the power spectral density (PSD) functions of streamwise velocity fluctuations u_1 and u_2 acquired simultaneously using two single Tungsten hotwires (Dantec 55P11) HT1 and HT2, respectively (Fig. 1(a)). While HT1 is located at the mid-gap ($L/2$), the HT2 in the wake with a streamwise distance of $2D$ from the downstream cylinder, both at a lateral distance of D from the wake-centre-line (Fig. 1(b)). The hotwires are translated in the spanwise direction for $1.19 \le L^* \le 4.05$, with $\Delta L^* = 0.16$. The signal is acquired at a sampling frequency of 3 kHz per channel for 30 s. The PSD functions (Eu) of u_1 and u_2 were calculated using

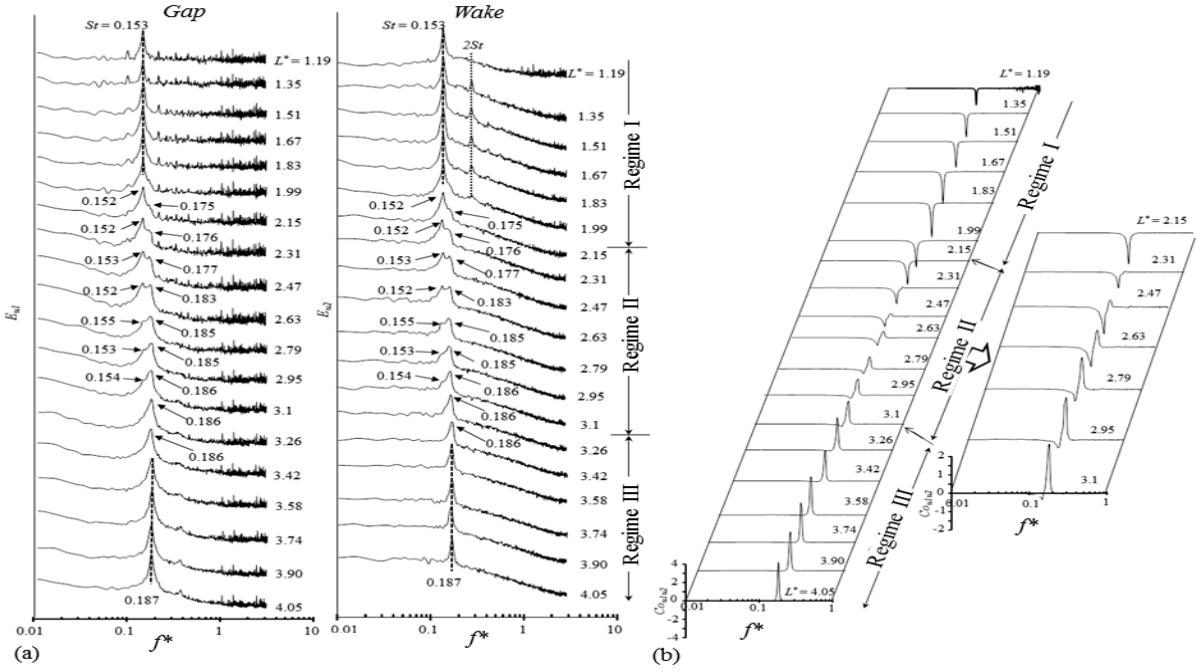

Figure 1 (a). PSD functions Eu_1 and Eu_2 of streamwise fluctuating velocities u_1 and u_2 captured simultaneously from HT1 and HT2, respectively and (b). Co-spectra Co_{u1u2} between u_1 and u_2.

a fast Fourier transform. The measured uncertainty in estimating *St* is estimated to be less than 2%.

Flow fields in the gap and wake in the *x*-*y* plane at different L^*, along the symmetric (*x, z*) plane ($y^* = 0$) for $1 \le L^* \le 4.05$ and in wake (*y, z*) plane for $1 \le L^* \le 2$ and $2.5 \le L^* \le 3.5$ were measured using a Dantec high-speed 2*D* PIV system. The flow was seeded with smoke particles with mean particle size of about 1 μm in diameter. The particle images are acquired using a dual-pulse laser source, a CMOS sensor based camera and a synchronizer. The PIV field of view for the gap flow measurement encompasses $x^* = -0.3$ to $L^* + 0.3$ and $y^* = -2.5$ to 2.5 (Fig. 1(b)) and that for the wake flow is $x^* = L^* - 0.3$ to $L^* + 5$ and $y^* = -2.5$ to 2.5 (Fig. 1(b)). An interrogation window of 32 × 32 pixel with an overlap of 50% in each direction is used for calculating the vector field. The spatial resolution of the vorticity data was 0.05*D*.

A surface-oil-flow visualization experiment was also conducted to capture the mean shear stress pattern including various singular points. A thin black film of 0.03 mm in thickness was wrapped on each cylinder and coated with a mixture of titanium dioxide and silicon oil. The cylinders were then installed in the wind tunnel, and the solution distribution on the cylinder surface was achieved after at least 20 minutes of exposure to the uniform flow in the wind tunnel. The black film was then unwrapped carefully, and photographs of solution distribution on the film were taken with a digital camera.

RESULTS

Vortex shedding and Strouhal number

Figure 2 shows the power spectral density (PSD) functions for both gap and wake, where *St* values, corresponding to the peaks are marked for each L^*. The power spectra have distinctive attributes at different flow regimes. The regime II features twin peaks whereas regimes I and III are characterized by a sharp peak for both E_{u1} and E_{u2}. A small peak at the second harmonic is an additional attribute for E_{u2} at regime I only. Regime I corresponds to $St = 0.153$ at both gap and wake, including the second harmonics of *St* at the wake only (Fig. 2(b)). This second harmonic peak is relatively strong at $L^* = 1.51$ - 1.67, diminishing at the lower ($L^* < 1.51$) and upper ($L^* > 1.67$) extremes of the regime. The appearance of the second harmonic is associated with the alternate reattachment of the upstream cylinder shear layers onto the downstream cylinder. The co-spectrum Co_{u1u2} (Fig. 4(b)) of u_1 and u_2 at regime I displays a negative peak bearing the signature that the upstream-cylinder shear layer reattachment and the shedding behind the downstream cylinder occur in an anti-phase fashion.

In regime II, two Strouhal numbers crop up; the corresponding peaks are closely spaced, yielding wideband frequency spectra. One (*St* = 0.152 - 0.155 depending on L^*) of the two Strouhal numbers is almost equal to the *St* (= 0.153) in regime I. The other *St* grows from 0.175 to 0.186 as L^* increases from 2.15 to 3.1. The latter value (= 0.186) is very close to the *St* (= 0.187) in regime III. The observation suggests two different flows (reattachment and coshedding) prevailing in regime II. The peak heights of the two Strouhal numbers change oppositely as L^* grows; the first *St* peak decays with L^* and the other peak matures. That is, the duration of the coshedding and reattachment flows broadens and shortens, respectively, as L^* extends from 2.15 to 3.1. The two peaks are nearly equal in height at $L^* = 2.63$, the two flows sharing the time almost 50% each. As such, Co_{u1u2} for $2.15 \le L^* \le 3.1$ in general shows a negative and a positive peak; while the negative peak dampens with L^*, the other boosts, both becoming almost similar in magnitude at $L^* =$

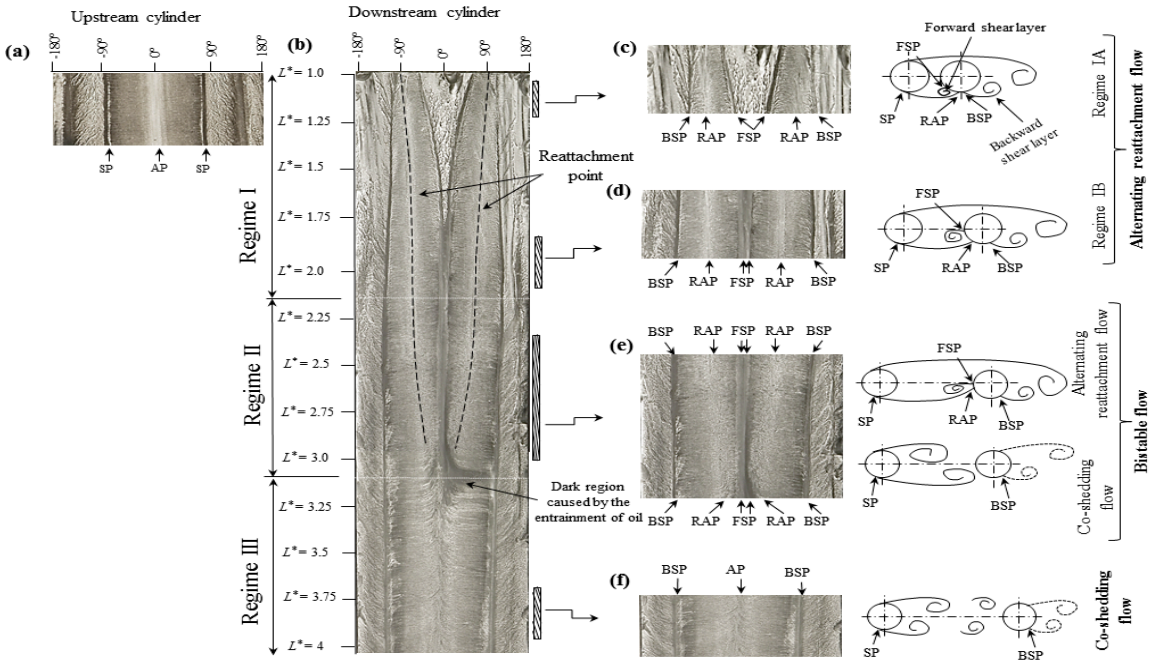

Figure 3. Surface oil flow print of (a) upstream cylinders, (b-f) downstream cylinder.

2.63. Unlike nonparallel cylinders, for parallel cylinders (e.g. Alam 2014), the bistable flow (regime II) appears for a very narrow range of L^* and the two St peaks are sharp and spaced. An increase in L^* to regime III ($L^* > 3.1$) leads to a single peak at $St \approx 0.186$, carrying only the higher St prevailing in regime II. The appearance of the single, sharp peak indicates that the flow is now the coshedding. The positive Co_{u1u2} peak in Fig. 2(b) indicates that for a given time the vortex shedding from the two cylinders occurs almost inpahse for $3.26 \leq L^* \leq 4.05$. $St = 0.186$ is observed at $L^* = 3.26$ and 3.42 which increases very slightly, $St = 0.187$ at $3.58 \leq L^* \leq 4.05$, while $St_o = 0.201$. That is, a large L^* is required for St to reach St_o for the nonparallel cylinders.

Surface and Spatial Flow Structure

Surface-oil-flow prints of the upstream and downstream cylinders are shown in Figs. 3(a) and 3(b), respectively. The surface print of the downstream cylinder is given for the entire span covering $L^* = 1.0$ to 4.05. Three singular lines, a front stagnation line/attachment line (AP, $\theta_{AP} = 0°$) and two separation lines (SP, $\theta_{SP} = \pm 78°$) are observed throughout the span for upstream cylinder; hence, only a small section of the surface print is presented (Fig. 3(a)). Many more lines on the surface print prevail for the downstream cylinder, and their angular positions vary with L^*, suggesting a significant change in the flow structure with L^* (Figs. 3(b)-3(f)). On the surface flow print of the downstream cylinder (Fig. 3(b)), six singular lines are observed at regime I ($1 \leq L^* < 2.15$), the six lines transmute to three lines at regime II ($2.15 \leq L^* \leq 3.1$, and the three lines persist at regime III ($L^* > 3.1$). Representative sections of the regimes and the corresponding sketches are presented in Fig. 3(c)-3(f). The reattachment point (RAP) of the upstream-cylinder-generated shear layer onto the downstream cylinder is marked with black dashed line along the span (Fig. 3(b)). Black dashed line marks the splitting of the reattaching shear layer into two flow streams, one flows forward (forward shear layer) and the other flows downstream (backward shear layer) along the cylinder surface (see the sketch in Fig. 3(c)) and separate from the cylinder surface at FSP (forward separation point) and BSP (backward separation point), respectively. The angular positions θ_{RAP}, θ_{FSP} and θ_{BSP} (not shown here) of RAP, FSP and BSP, respectively, are observed dependent on L^*. In order to strengthen the discussion on the flow at each regime, PIV-measured instantaneous vorticity fields are presented in Fig. 4.

Alternating reattachment flow ($1 \leq L^* < 2.15$). From Fig. 3(b), in this regime the upstream cylinder shear layer reattaches on the downstream cylinder with the reattachment position moving forward (θ_{RAP} reduces) almost linearly with L^*. The linearity arises due to a spanwise interaction of the flows at continuously varied L^*. As L^* increases from 1.0 to 2.15, while θ_{FSP} wanes sharply (from 55° to 5°), θ_{BSP} grows gradually (from 107° to 121°). A total of six singular lines, two RAP, two BSP and two FSP emerge on the downstream cylinder surface print for $1 \leq L^* < 2.15$ (Fig. 3(b)). This regime may be divided into two sub-regimes labeled with IA and IB, respectively (Figs. 3(c)-3(d)). At regime IA ($1 \leq L^* \leq 1.6$), FSP rapidly moves forward (θ_{FSP} reduces exponentially) and BSP slowly moves backward (θ_{BSP} linearly increases).

On the other hand, at regime IB ($1.6 < L^* < 2.15$), FSP gently moves forward and approaches the nominal forward stagnation line, and BSP moving backward at a higher rate compared to that at regime IA reaches the maximum value (121°) at $L^* \approx 2.15$. Throughout $1 \leq L^* < 2.15$, RAP shifts forward almost linearly until it reaches the mid position ($\theta_{RAP} = 62°$) between FSP ($\theta_{FSP} = 5°$) and

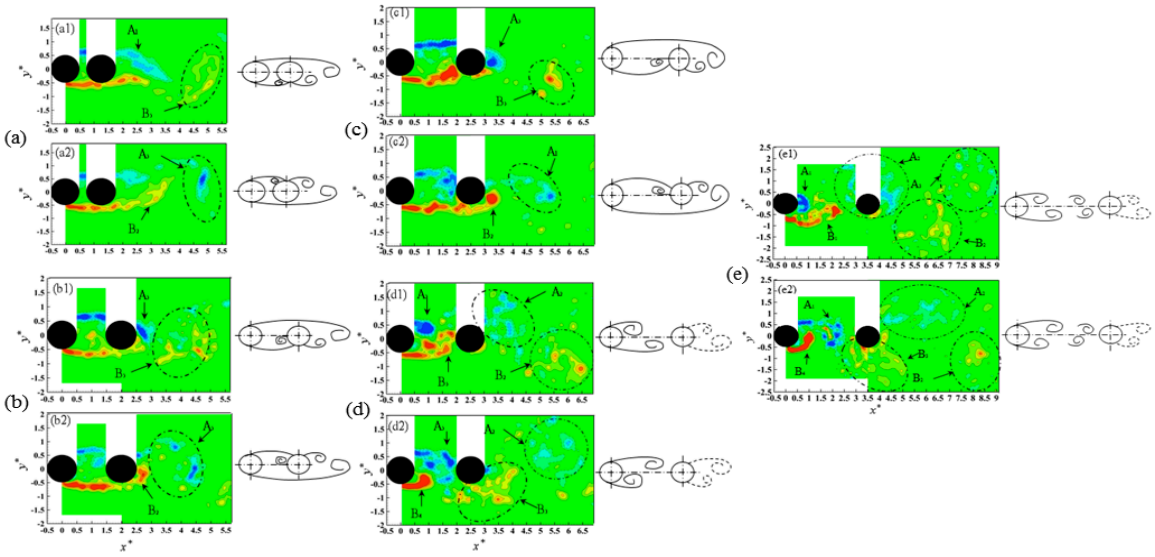

Figure 4. Instantaneous vorticity contours and incurred flow patterns obtained from PIV at, (a) $L^* = 1.25$, (b) $L^* = 1.5$, (c,d) $L^* = 2.5$, (d) $L^* = 3.5$

BSP ($\theta_{BSP} = 121°$) at $L^* = 2.15$. In regime IA (Fig. 4(a1))

high momentum fluid in the shear layer largely follows the backward shear layer and shed vortices in the wake, while a very small amount of the fluid recirculates in the gap. On the other hand, in regime IB (Fig. 4(a2)), the large quantity of the high momentum fluid recirculates in the gap with reattachment point moving forward. The high momentum fluid largely follows the forward shear layer, the backward shear layer rolls very close to the rear surface of the downstream cylinder.

Bistable flow ($2.15 \le L^* < 3.1$). Both reattachment and coshedding flows appear intermittently, with dominance shifting from one to other respectively, with increasing or decreasing L^* from $2.15 \le L^* \le 3.1$ (similar to observed in frequency spectrum, Fig. 2(a)). *RAP* line gets faint with increasing L^* and destroyed completely at $L^* = 2.9$ (Fig. 3(b)) due to the dominance of the coshedding flow. With L^*, the θ_{RAP} rapidly changes, moving toward the nominal front stagnation point. The θ_{FSP} does not change much, remaining very close to the nominal front stagnation point throughout the L^* range. On the other hand, the *BSP* starts moving forward (θ_{BSP} reduces) from the maximum value ($\theta_{BSP} = 121°$ at $L^* = 2.25$). Instantaneous vorticity structures (Figs. 4(c-d)) display two different types of flow patterns at the same L^*. One is the reattachment flow qualitatively similar to that in regime IB (Fig. 4(b)) and the other resembles the co-shedding flow in regime III (Fig. 4(e)). As θ_{RAP} is smaller than that in regime IB, more fluid can go into the gap region (Fig. 4(c)). In the second flow pattern the alternate vortex shedding from the upstream cylinder, similar to what was observed for the downstream cylinder only (Fig. 4(d)), is also initiated. Due to the existence of two stable flow patterns, the flow is categorized as bistable (*BS*) flow and labeled as regime II in Fig. 3(e) and Figs. 4(c-d).

Coshedding flow ($L^* > 3.1$). Vortex shedding occurs from the individual cylinders. That is, only the second flow pattern in regime II continues to appear in regime III. The oil-flow pattern (Fig. 3(f)) is similar to that on the upstream cylinder (Fig. 3(a)), both having one *AP* and two *BSP*. The instantaneous vorticity patterns shown in Fig. 4(e) illustrate alternate vortex shedding from each cylinder.

Overall each regime has distinct features associated with singular points. Regime IA is connected with a swift forward movement of the *FSP*, regime IB features the increase in *BSP* until it approaches the maximum value, regime II is linked with a rapid forward movement of *RAP* and an almost invariant *FSP*. Regime III is characterized by the absence of *RAP* line. Bistable flow appears in a larger range of L^* ($2.15 \le L^* \le 3.1$) but at a smaller L^* compared to that for parallel cylinders.

Flow Topology

PIV measurements are also conducted in the gap and wake regions at the wake centerline plane (*x-z* plane at $y^* = 0$) for $1 \le L^* \le 4.05$ (Fig. 5(a)) and in *y-z* plane (Fig. 5(b)) for $1.0 \le L^* \le 2.0$, and $2.5 \le L^* \le 3.5$ in the wake region. Total 1500 images at a sampling frequency of 600 Hz are captured for the measurements in both *x-z* and *y-z* planes.

In the time mean streamlines in *x-z* plane (Fig. 5(a)) a separatrix in the gap, representing the trace of the saddle points along the span, is observed at regime III. The separatrix at regime III shifts upstream with an increase in L^*. Remarkably, the flows before and after the separatrix in the plane through the centerline are directed toward the

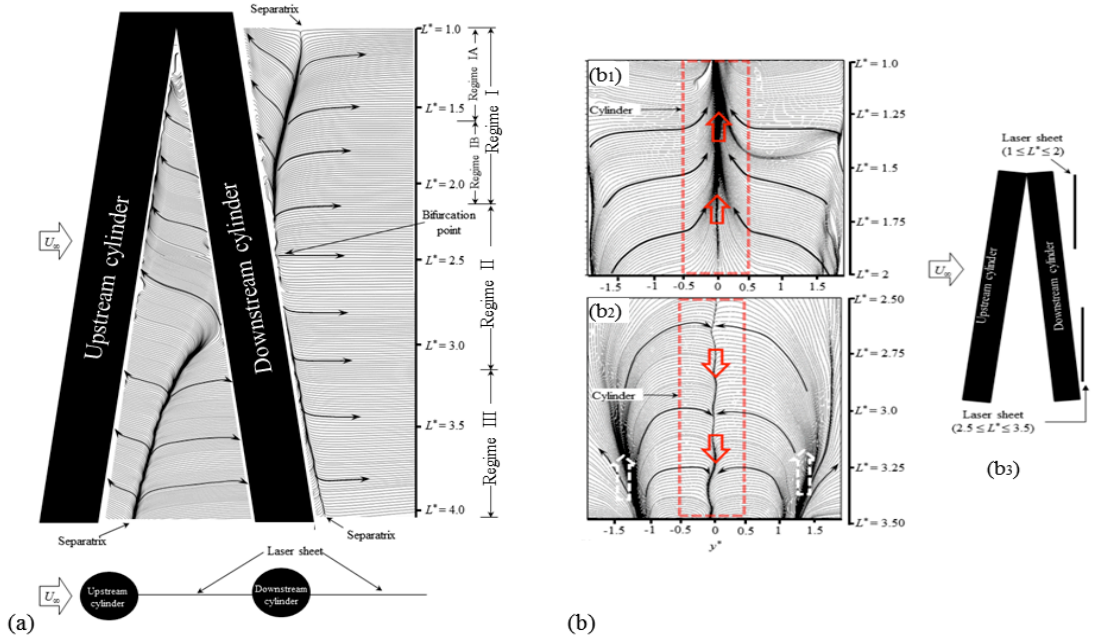

Figure 5. Time averaged streamlines in (a) *x-z* plane, (b) *y-z* plane.

upstream and downstream cylinders, respectively, both inclined upward with respect to the free stream. As the streamlines start at the separatrix and end at the rear and forward stagnation points of the upstream and downstream cylinders, respectively, this inclination is considered to be the angle between the free stream and the line connecting two end points for a streamline in the *x-z* plane. The inclination of the flow directed toward the downstream cylinder is smaller than that toward the upstream cylinder. The separatrix extends into regime II, becoming wider as it tends to touch the downstream cylinder at $L^* \approx 2.9$ corresponding to the dark region at the *FSP* in the surface oil print of the downstream cylinder (Fig. 3(b)). The extension of the separatrix into regime II is due to the dominance of the coshedding flow at a higher L^* in regime II. The streamline at $L^* < 2.9$, being inclined upward, are directed toward the upstream cylinder.

Compared to that in the gap, the streamline pattern in the wake region (Fig. 5(a)) displays different scenarios: the flow at small L^* ($1 \le L^* < 2.5$) is inclined upward, towards the small L^*, alike the gap flow; and that at large L^* ($2.45 < L^* \le 4.05$) is inclined downward, towards the large L^*, opposite to that in the gap region.

Therefore, the flow at $L^* \approx 2.5$ dividing the two L^* ranges (bifurcation point, Fig. 5(a)) is parallel to the freestream flow. As the vortex shedding occurs from the downstream cylinder regardless of flow regimes, the separatrix materializes for the entire span of the cylinder. It is conspicuous that the streamwise separation of the wake separatrix from the cylinder center is smallest at the bifurcation L^* (= 2.5). It grows as L^* is decreased or increased from the bifurcation L^*; the growth is, however, larger for the former. Figure 5(b1) and 5(b2) presents the instantaneous contours of the streamwise vorticity ω_x^* (= $\omega_x D/U_\infty$) superimposed with velocity vectors in the *y-z* plane for small ($1.0 \le L^* \le 2.0$) and large ($2.5 \le L^* \le 3.5$) spacing, respectively. In both cases, the flow corresponds to the vortex shedding from the left side of the cylinder. In the *x-z* plane (Fig. 5), it is observed that the reversed flow behind the downstream cylinder exhibits a spanwise movement towards the small L^* for $1.0 \le L^* \le 2.0$ but towards the large L^* for $2.5 \le L^* \le 3.5$. Accordingly, the corresponding time-averaged streamlines around $y^* = 0$ (Fig. 5(b1)) are always directed towards the small L^* for $1.0 \le L^* \le 2.0$ behind the downstream cylinder (Fig. 5(a)). For the coshedding flow, as observed in Fig. 4(d) and 4(e), the impinging vortex upon the downstream cylinder spreads laterally outwards, and only part of this vortex contiguous to the cylinder follows the shear layer of the downstream cylinder. This lateral spread of the incoming vortices from the upstream cylinder thus greatly influences the vortex shedding from the downstream cylinder. The time-averaged flow field in Fig. 5(b2) shows that the flow about the symmetric plane ($y^* = 0$) turns downward, consistent with the observation from Fig. 5(a), but the flow away from the symmetric plane is upward-directed, as indicated by the white dashed arrows in Fig. 5(b2)), following the upstream cylinder spiral vortex.

In other words, the Karman vortex shedding from the downstream cylinder itself engulfs the free-stream fluid, a small part of it turning downward and the rest upward. Two regions of closely separated streamlines are observed around $y^* \approx (1.2\text{-}1.5)$, depending on L^*, where the flow is largely upward, connected to the core of the spiral vortex from the upstream cylinder.

CONCLUSIONS:

Three distinct flow regimes for two nonparallel cylinders are observed. Regime I (alternate reattachment, $1 \le L^* < 2.15$) is featured by alternating reattachment of the upstream-cylinder shear layers onto the downstream cylinder, quasi-steady vortex in the gap, six singular lines (two *RAP*, two *BSP* and two *FSP*) on the downstream cylinder surface, and alternate shedding from the downstream cylinder. Regime II (bistable flow, $2.15 \le L^* \le 3.1$) is a transition regime, characterized by both alternate reattachment and coshedding flows that occur intermittently, where the six singular lines transmute to three. Due to the intermittent presence of reattachment and coshedding flows, jump in *St* prevails. Regime III (coshedding, $3.1 < L^* \le 4.05$) portraits three singular lines (one *AP* and two *BSP*). *St* at regime III for both nonparallel and parallel cylinders are comparable to each other.

Flow in the gap is inclined upward, toward the small L^* for all regimes. So is flow behind the downstream cylinder for $1 \le L^* < 2.5$ (regime I and reattachment-dominated flow in regime II), but opposite for $2.5 < L^* \le 4.05$ (regime III and coshedding dominated flow in regime II). The upward and downward directed spiral vortices behind the downstream cylinder are separated by a bifurcation point at $L^* = 2.5$.

REFERENCES

Alam, M. M., Moriya, M., Takai, K., Sakamoto, H., 2003, "Fluctuating fluid forces acting on two circular cylinders in a tandem arrangement at a subcritical Reynolds number", *Journal of Wind Engineering & Industrial Aerodynamics*, Vol. 91, pp. 139-154

Alam, M. M., 2014, "The aerodynamics of a cylinder submerged in the wake of another", *Journal of Fluids and Structures*, Vol. 51, pp. 393-400.

Alam, M. M., 2016, "Lift forces induced by the phase lag between the vortex sheddings from two tandem bluff bodies", *Journal of Fluids and Structures*, Vol. 65, pp. 217-237.

Hogan, J. D., Hall, J. W., 2011, "Experimental study of pressure fluctuations from yawed circular cylinders", *AIAA Journal*, Vol. 49, pp. 2349-2356

Igarashi, T., 1981, "Characteristics of the flow around two circular cylinders arranged in tandem (first report)", *Bulletin of JSME*, Vol. 24, pp. 323-331.

Lam, K., Lin, Y. F., Zou, L., Liu, Y., 2012, "Numerical simulation of flows around two unyawed and yawed wavy cylinders in tandem arrangement", *Journal of Fluids and Structures*, Vol. 28, pp. 135-151.

Ming, Z., Liang, C., Tong M. Z., 2009, "Direct numerical simulation of three-dimensional flow past a yawed circular cylinder of infinite length", *Journal of Fluids and Structures*, Vol. 25, pp. 831-847.

Najafi, L., Firat, E., Akilli, H., 2016, "Time-averaged near-wake of a yawed cylinder", *Ocean Engineering*, Vol. 113, pp. 335-349.

Sakamoto, H., Haniu, H., Obata, Y., 1987, "Fluctuating forces acting on two square prisms in a tandem arrangement", *Journal of Wind Engineering and Industrial Aerodynamics*, Vol. 26, pp. 85–103.

Stephen, J. W., James, D. H., Joseph, W. H., 2013, "Vortex shedding in a tandem circular cylinder system with a yawed downstream cylinder", *Journal of Fluids Engineering*, Vol. 135, pp. 071202-(1-7).

Stephen, J. W., Joseph, W. H., 2013, "Experimental Investigation of a tandem cylinder system with a yawed upstream cylinder", *Journal of Fluids Engineering*, Vol. 136, pp. 011302-(1-8).

Xu, G., Zhou, Y., 2004, "Strouhal numbers in the wake of two inline cylinders", *Experiments in Fluids*, Vol. 37, pp. 248–256.